Check for updates

Distance-based paper microfluidic devices for rapid visual quantification of heavy metals in herbal supplements and cosmetics†

Yanawut Manmana,[ab] Mirek Macka [ID] [bcd] and Nantana Nuchtavorn [ID] *[a]

Distance-based detection (DbD) on paper-based microfluidic analytical devices (µPADs) has emerged as a promising, cost-effective, simple, and instrumentation-free assay method. Broadening the applicability of a new way of immobilization of reagent for DbD on µPADs (DµPADs) is presented, employing an ion exchange (IE) interaction of an anionic metallochromic reagent, 2-(5-bromo-2-pyridylazo)-5-[*N-n*-propyl-*N*-(3-sulfopropyl)amino]phenol (5-Br-PAPS), on the anion-exchange filter paper. The IE DµPADs demonstrate superiority over standard cellulose filter paper in terms of the degree of reagent immobilization, detection sensitivity, and clear detection endpoints due to the strong retention of 5-Br-PAPS. The study investigated various parameters influencing DbD, including 5-Br-PAPS concentrations (0.25–1 mM), buffer types (acetic acid–Tris, MES), buffer concentrations (20–500 mM), and auxiliary complexing agents (acetic, formic, and glycolic acids). Subsequently, the performance of 17 metals (Ag$^+$, Cd^{2+}, Co^{2+}, Cr^{3+}, Cu^{2+}, Fe^{2+}, Hg^{2+}, La^{3+}, Mn^{2+}, Ni^{2+}, Pb^{2+}, Ti^{2+}, Zn^{2+}, Al^{3+}, As^{3+}, Fe^{3+}, and V^{4+}) was evaluated, with color formation observed for 12 metals. Additionally, the paper surface was examined using SEM and SEM-EDX to verify the suitability of certain areas in the detection channel for reagent immobilization and metal binding. This method demonstrates quantitation limits of metals in the low µg mL^{-1} range, showing great potential for the rapid screening of toxic metals commonly found in herbal supplements and cosmetics regulated by the Food and Drug Administration (FDA). Thus, it holds promise for enhancing safety and regulatory compliance in product quality assessment. Furthermore, this method offers a cost-effective, environmentally sustainable, and user-friendly approach for the rapid visual quantification of heavy metals for in-field analysis, eliminating the need for complex instrumentation.

1. Introduction

Heavy metals are significant environmental contaminants, with trace levels of exposure capable of eliciting harmful effects in plants, animals, and humans, leading to multiple organ damage. Humans are exposed to heavy metals through ingestion or consumption of contaminated food or water, inhalation from atmospheric sources, and skin contact in agriculture, pharmaceutical, manufacturing, residential, and industrial areas. Notably, various heavy metals including arsenic (As), cadmium (Cd), lead (Pb), and mercury (Hg) are associated with high degrees of human poisoning and are of significant concern. These heavy metals can accumulate in tissues over time, disrupting cellular functions and leading to neurotoxicity, hepatotoxicity, nephrotoxicity, and increased risks of cancer. These metals can interfere with cellular metabolism by binding to proteins and enzymes, impairing their normal activity. Conversely, heavy metals such as cobalt (Co), copper (Cu), chromium (Cr), iron (Fe), magnesium (Mg), manganese (Mn), nickel (Ni), and zinc (Zn) serve as essential nutrients, playing crucial roles in various biochemical and physiological functions.[1,2] Therefore, efficient, reliable, and sensitive analytical methods are required for monitoring heavy metal contamination, assessing exposure levels, and determining the content of essential metals. Numerous analytical methods have been reported for the determination of heavy metals in various matrices. For instance, the United States Pharmacopeia recommends inductively coupled plasma-atomic (optical) emission spectroscopy (ICP-AES or ICP-OES) or ICP-mass spectroscopy for analysis of elemental impurities in drug products and dietary supplements.[3] The United States Environmental Protection Agency (EPA) suggests ICP-AES analysis of metal elements in water and waste matrices.[4] Additionally, the

[a]Department of Pharmaceutical Chemistry, Faculty of Pharmacy, Mahidol University, 447 Sri-Ayudhaya Rd., Rajathevee, Bangkok 10400, Thailand. E-mail: nantana.nuc@mahidol.edu

[b]School of Natural Sciences and Australian Centre for Research on Separation Science (ACROSS), University of Tasmania, Private Bag 75, Hobart 7001, Australia

[c]Department of Chemistry and Biochemistry, Mendel University in Brno, Zemedelska 1, CZ-613 00 Brno, Czech Republic

[d]Central European Institute of Technology, Brno University of Technology, Purkynova 123, CZ-612 00 Brno, Czech Republic

International Organization for Standardization (ISO) utilizes ICP-MS for measuring traces of heavy metals in finished cosmetic products.[5] Although the ICP technique is known for its sensitivity, specificity, and accuracy in determining heavy metal at trace levels, this method is expensive and requires benchtop instruments in the laboratory, as well as highly trained staff to operate.[6] Consequently, there is an ongoing effort to develop cost-effective, user-friendly, and environmentally friendly alternatives.

Microfluidic paper-based analytical devices (μPADs) have been developed as simple, cheap, and disposable alternatives to conventional detection techniques. The fabrication of μPADs involves patterning the hydrophobic barrier on the hydrophilic paper.[7] A wide variety of detection methods on μPADs have been reported for the measurement of various analytes in several matrices such, as colorimetry,[8–10] fluorescence,[11,12] and electrochemistry.[13] Detection of heavy metals on μPADs has been accomplished by several detection methods (Table 1). Among these methods, distance-based detection (DbD) stands out as an instrumentation-free quantitative detection technique. The signal length developing on the channel is proportional to the analyte's concentration, which can be observed by the naked eye using a printed scale along the detection channel.[33–35]

Therefore, the integration of DbD with μPADs (DμPADs) represents a promising technique for in-field analysis, particularly resource-limited areas. A previous report evaluated the fluidic properties of ion exchange (IE) paper and examined the effects of pH and ionic strength on the displacement of deposited reagents. This study also assessed the measurement of Ca^{2+} in serum and total acidity in wine.[36] In this work, we have significantly extended the applicability of DμPADs by employing IE paper for the rapid screening of metal ions. Unlike other works, we utilized an anionic metallochromic reagent, 2-(5-bromo-2-pyridiylazo)-5-[N-n-propyl-N-(3-sulfopropyl)amino]phenol (5-Br-PAPS), which is strongly immobilized on IE paper through IE interaction This approach avoids the need for complex synthesis or surface modifications while enabling reaction with a broad range of heavy metals of toxicological or environmental concern.

Various factors influencing the metal-5-Br-PAPS complex formation on the IE paper were investigated, including a concentration of buffer, the concentration of 5-Br-PAPS, and types of complexing reagents. Under optimal conditions, a clear detection endpoint and accurate signal readout of 12 metal ions among 17 metal ions (i.e., Ag^+, Cd^{2+}, Co^{2+}, Cr^{3+}, Cu^{2+}, Fe^{2+}, Hg^{2+}, La^{2+}, Mn^{2+}, Ni^{2+}, Pb^{2+}, Ti^{2+}, Zn^{2+}, Al^{3+}, As^{3+}, Fe^{3+}, and V^{4+}) were observed. Furthermore, harmful heavy metals, as regulated by the Food and Drug Administration (FDA), were also tested in real samples such as dietary supplements and cosmetics, demonstrating the practical applicability and robustness of the approach.

Additionally, the method was assessed with the criteria derived from the 12 principles of green analytical chemistry, achieving an impressive Analytical GREEnness (AGREE) score of 0.65 (Fig. S1†).[37] Compared to existing methods for heavy metal ion detection using μPADs (Table 1), the developed devices provide a detection range comparable to those reported in the literature. While certain techniques achieve lower detection limits, this approach offers the distinct advantage of straightforward fabrication, eliminating the need for complex chemical modifications or specialized probe synthesis. By incorporating IE paper with 5-Br-PAPS, the device enables instrumentation-free detection, facilitating rapid screening of several heavy metals. Although the use of a single complexometric dye to detect multiple metals may compromise specificity, this limitation can be addressed through additional targeted steps to enhance selectivity for specific metal ions.

2. Experimental

2.1. Chemicals

ICP standard solutions of arsenic (As), cadmium (Cd), lead (Pb), and silver (Ag), were obtained from Accustandard® (Connecticut, USA). ICP standard solutions of aluminum (Al), chromium (Cr), copper (Cu), lanthanum (La), mercury (Hg), titanium (Ti), vanadium (V), and zinc (Zn) were purchased from TraceCERT®, Sigma-Aldrich (Missouri, USA). Ferrous sulfate (Fe^{2+}), formic acid, and ICP standard solution of manganese (Mn) and nickel (Ni) were purchased from Ajax Finechem (New South Wales, Australia). ICP standard solutions of cobalt (Co) and iron (Fe) were purchased from BDH Chemical (Poole, UK). Tris(hydroxymethyl)aminomethane (Tris) was purchased from Mallinckrodt (Staines-upon-Thames, UK). Sodium chloride (NaCl), sodium hydroxide (NaOH), 2-(N-morpholino)ethanesulfonic acid (MES), 3-(N-morpholino)propanesulfonic acid (MOPS), and glycolic acid were purchased from Sigma-Aldrich (Missouri, USA). Acetic acid was obtained from Merck (Darmstadt, Germany), and disodium 5-Br-PAPS·2H₂O was purchased from Supelco® (Missouri, USA). Whatman® filter paper No.1, 42, and DE 81 were supplied by GE Healthcare Life Sciences (Chicago, USA).

2.2. Preparation of reagent, standard, and sample solutions

The stock solution of 5-Br-PAPS was prepared by dissolving 8 mg of 5-Br-PAPS in 5 mL deionized (DI) water. Stock metal solutions of 1000 μg mL^{-1} in 2–5% HNO_3 were further diluted to the desired concentration with 2% HNO_3. A Tris solution was prepared by dissolving 3.02 g of Tris in 5 mL DI water to obtain 5 M Tris solution. Subsequently, a 500 mM acetic acid–Tris buffer solution was prepared by transferring 0.5 M acetic acid into a 10 mL volumetric flask and adjusting the pH using a 5 M Tris solution. Additionally, a 250 mM MOPS buffer was prepared by transferring 0.523 g of MOPS into a 10 mL volumetric flask and adjusting the pH using 5 M sodium hydroxide. Similarly, a 250 mM MES buffer was prepared by dissolving 0.488 g of MES in a 10 mL volumetric flask and adjusting the pH using 2 M HNO_3.

Artificial seawater and salt lake solutions with NaCl concentrations ranging from 10 to 600 mM were prepared by dissolving the appropriate amount of NaCl in DI water.[38] Standard solutions of Zn^{2+} and Co^{2+}, as model analytes, were then spiked at concentrations of 4 and 6 μg mL^{-1}, respectively, to study the effect of salt on metal analysis on the DμPADs.

Table 1 Paper-based microfluidic analytical devices for determination of heavy metals

Heavy metal	Detection method	Detection probe	Type of paper	Sample matrix	Detection range	Ref.
Cd^{2+}, Co^{2+}, Cu^{2+}, Fe^{3+}, Hg^{2+}, La^{3+}, Ni^{2+}, Pb^{2+}, Zn^{2+}, As^{3+}, and V^{4+}	DbD	5-Br-PAPS	IE paper	Herbal supplements and cosmetics	2–20 ppm	Proposed study
Pb^{2+}	DbD	G-quadruplex/hemin DNAzyme and 3,3,5,5-tetramethyl benzidine	Standard cellulose paper (grade 1 with 11 μm pore size and 180 μm thickness)	Milk	0.02–50 μM	14
Cu^{2+} and Fe^{3+}	Color intensity of fluorescence image	Fluorescent metal-organic framework@tetracycline	Standard cellulose paper	Drinking water	0.1–80 μM Cu^{2+}; 0.2–160 μM Fe^{3+}	15
Fe^{2+} and Fe^{3+}	Color intensity	Bathophenanthroline (probe) and hydroxylamine (reducing agent)	Standard cellulose paper	White and red wines	0.25–2.5 ppm	16
Ni^{2+}, Fe^{3+}, and Cu^{2+}	Color intensity	Dimethylglyoxime, bathophenanthroline, and bathocuproine, respectively	Standard cellulose paper	Drinking, and river water	1–50 ppm Ni^{2+}; 0.5–15 ppm Fe^{3+}; 0.10–5 ppm Cu^{2+}	17
Pb^{2+} and Hg^{2+}	Color intensity of fluorescence image	Aptamer integrated upconversion nanoparticles	Nitrocellulose membrane	Tap and pond water	5–1000 nM Pb^{2+}; 25–5000 nM Hg^{2+}	18
Pb^{2+}	Potentiometric detection	Ion-selective electrode	Gold modified on both sides of cellulose paper grade 388 (10–15 μm pore size and 210 μm thickness)	Simulated environmental samples	10 μM–6.3 mM	19
Cu^{2+}, Fe^{3+}, and Hg^{2+}	Color intensity	Graphene quantum dots	Standard cellulose paper	Urine	0.001–5 ppm	20
Cu^{2+}	Color intensity of fluorescence quenching image	6-Mercaptonicotinic acid and L-cysteine decorated zinc-doped carbon dots	Surface modification of standard cellulose paper with zinc-doped carbon dots through amide bond	Environment water	0.1–60 ppm	21
Pb^{2+}	Electrochemiluminescence detection	Pb^{2+}-specific DNAzymes	Gold nanoparticles modified cellulose paper grade 2 (>8 μm pore size and 190 μm thickness)	—	0.01–50 nM	22
Cu^{2+}, Co^{2+}, Ni^{2+}, Hg^{2+}, and Mn^{2+}	Color intensity	Bathocuproine, 4-(2-pyridylazo) resorcinol, dimethylglyoxime, and dithizone	Standard cellulose paper	Drinking, tap, and pond water	0.3–63.6 ppm Cu^{2+}; 0.6–4.7 ppm Co^{2+}; 5.9–352.2 ppm Ni^{2+}; 0.2–12.04 ppm Hg^{2+}; 0.1–0.6 ppm Mn^{2+}	23
Cu^{2+}, Cd^{2+}, Pb^{2+}, and Hg^{2+}	Color intensity of fluorescence image	Ion imprinted polymer grafted CdTe quantum-dots	Standard cellulose paper and glass fiber paper	Seawater	0.007–0.015 ppm	24
Ag^+	DbD	Gold nanoparticles	Gold nanoparticles modified standard cellulose paper	Drinking water	1–100 ppm	25

Table 1 (Contd.)

Heavy metal	Detection method	Detection probe	Type of paper	Sample matrix	Detection range	Ref.
Cd^{2+}, Pb^{2+}	Color intensity of fluorescence image	Ion imprinted polymer ZnSe quantum-dots	Standard cellulose paper and glass fiber paper	Seawater and lake water	1–70 ppm 1–60 ppm	26
Fe^{3+}, Ni^{2+}	Color intensity	1,10-Phenanthroline and dimethylglyoxime	Standard cellulose paper	River water	0.1–5 mM 1–50 mM	27
Cu^{2+}	DbD	Sodium diethyldithiocarbamate	Standard cellulose paper	Soil	1–100 ppm	28
Ni^{2+}, Cr^{4+}, and Hg^{2+}	Color intensity	Dimethylglyoxime, 1,5-diphenylcarbazide, and Michler's thioketone, respectively	Functionalization of NH_2, COOH, and SH on standard cellulose paper using silane compounds	Lake water	0.2–20 ppm	29
Cu^{2+}, total Fe, and Zn^{2+}	DbD	Zincon, bathophenanthroline, and dithizone, respectively	Cellulose filter paper grade 4 (20–25 μm pore size and 210 μm thickness)	Mining water	0.1–20 ppm	30
Hg^{2+}	DbD	Dithizone	Standard cellulose paper	Whitening cream	1–30 ppm	31
Ni^{2+}, Fe^{2+}, and Cu^{2+}	DbD	Dimethylglyoxime, bathophenanthroline, and dithiooxamide, respectively	Standard cellulose paper	Stainless steel	1–65 ppm	32

Three different brands of herbal capsules (brand A containing *Houttuynia cordata* and *Andrographis paniculata*, brand B containing *Momordica charantia*, and brand C containing *Coix lacryma-jobi*, *Cinnamomum cassia*, *Lycium chinense*, *Cuscuta chinensis*, *Ziziphus jujuba*, *Dioscorea opposita*, *Epimedium grandiflorum*, *Cordyceps sinensis*, *Schisandra chinensis*, and *Atractylodes macrocephala*) were collected from markets in Bangkok, Thailand. The cosmetic cream base was initially formulated by separately preparing ingredients in phase A and phase B (Table S1†) in beakers and heating them to 75 °C and 70 °C, respectively. These 2 phases of ingredients were mixed by a homogenizer at 4000 rpm and a temperature of 50–55 °C until the cream base was homogeneous. Then, the ingredient in phase C was gently added and thoroughly mixed until the temperature decreased to 35 °C.

All samples, including herbal supplements and cosmetics, were digested in 9 mL of a freshly prepared acid mixture of 65% HNO_3 and 37% HCl (1 : 3). The mixture was then gently boiled over a water bath at 95 °C until the samples were completely dissolved. To prevent sample loss, the inner walls of the beakers were washed with 10 mL DI water during the digestion process. Subsequently, the samples were filtered with Whatman® No. 42 filter paper (2.5 μm particle retention) and adjusted to a volume of 50 mL with DI water.[34] The herbal supplements were analyzed by ICP-OES, and samples without metal contamination were used as metal-free controls.

2.3. Fabrication of DμPADs

The shaped patterns of DμPADs, featuring a measuring scale with 1 mm intervals among the scale bars, were designed and printed on standard cellulose paper (Whatman No. 1, pore size of 11 μm and thickness of 180 μm) and IE paper (Whatman DE 81 anion exchanger, diethylaminoethyl cellulose paper with thickness of 230 μm) using a wax printer (Fuji Xerox ColorQube 8870 printer, Bangkok, Thailand). Circles of the sample application zone were then cut out, and the wax lines were melted to form a hydrophobic pattern of fluidic channels. Next, the paper with the patterned microfluidic channels was aligned with a pre-cut laminating film and laminated at 160 °C. Finally, a 5-Br-PAPS solution was deposited onto the detection zone.

Three-dimensional (3D) models of DμPAD cassettes were designed using the Fusion 360 academic version. The STL file format of the 3D model was then transmitted to the 3D printer software (Flashforge Guider IIs) and printed using a nozzle diameter of 0.3 mm, utilizing polylactic acid (PLA) filament with a diameter of 1.75 mm.[39] Each DμPAD was fixed on the cassette bed using double-sided adhesive tape at the corners (Fig. 1).

2.4. Study of factors affecting the metal ion analysis on DμPADs

Initially, DμPADs were fabricated using standard cellulose and IE papers. Then, 1.5 μL of 1 mM 5-Br-PAPS in 0.25 M MOPS buffer pH 7.0 was deposited on the detection channel. After the reagent dried under ambient conditions, 5 μL of 1–4 μg per mL Zn^{2+} were added to the sample reservoir, and the signal readout was observed after 15 min. Furthermore, parameters affecting
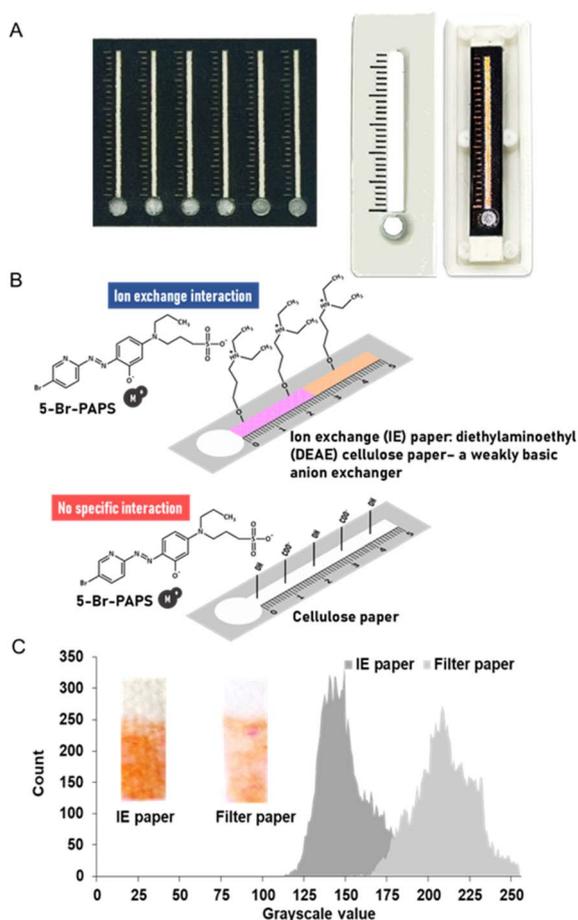
Fig. 1 The DµPADs for the measurement of heavy metals. (A) The DµPADs on IE paper and cassette fabricated by printing methods (B) The proposed interactions between 5-Br-PAPS deposited on anion exchange paper and standard cellulose filter paper and their metal complex formation (*M$^+$: metal ion and 5-Br-PAPS: 2-(5-bromo-2-pyridiylazo)-5-[N-n-propyl-N-(3-sulfopropyl)amino]phenol, disodium salt) (C) Histogram of color intensity of 5-Br-PAPS immobilized on cellulose and IE paper after immersion in water for 5 min.

the DbD of metal ions were investigated, including the concentrations of buffer (10–100 mM and 20–500 mM for acetic acid and acetic acid–Tris, respectively), the concentration of 5-Br-PAPS (0.25–1 mM in 250 mM acetic acid–Tris and MES–nitric acid buffer system), and types of auxiliary complexing agents (250 mM MES, 250 mM MES and 10 mM acetic acid, 250 mM MES and 10 mM formic acid, and 250 mM MES and 10 mM glycolic acid). The color intensity and length of color changes of model metal ions *i.e.*, Co^{2+}, Cu^{2+}, Ni^{2+}, Zn^{2+} at the concentration of 4 µg mL^{-1}, were determined. Subsequently, screening tests were conducted on DµPADs for a total of 17 metal ions (*i.e.*, Ag$^+$, Cd^{2+}, Co^{2+}, Cr^{3+}, Cu^{2+}, Fe^{2+}, Hg^{2+}, La^{2+}, Mn^{2+}, Ni^{2+}, Pb^{2+}, Ti^{2+}, Zn^{2+}, Al^{3+}, As^{3+}, Fe^{3+}, and V^{4+}).

Furthermore, the morphological characteristics of the IE paper and the predeposition of 5-Br-PAPS and subsequent metal binding onto its surface were examined using a scanning electron microscope (SEM) operating at 10 kV with a 3000 magnification. Elemental analysis was then performed at a voltage of 15 kV with a magnification of 3000×, employing

a SEM-energy dispersive X-ray spectrometer (SEM-EDX) (JEOL JSM-IT500HR, JED-2300, Missouri, USA). Additionally, the infrared (IR) spectra were collected using an iS5 Fourier transform IR (FT-IR) spectrometer with iD7 attenuated total reflection (ATR) (ThermoFisher Scientific, Massachusetts, USA).

2.5. Method validation

The proposed method was validated following the guidelines of the Association of Official Analytical Chemists (AOAC), encompassing assessments of linearity, precision, accuracy, and limit of quantitation (LOQ).[40] Calibration curves of Co^{2+}, Cu^{2+}, Fe^{3+}, V^{4+}, and Zn^{2+} were established by plotting the distance of color change against five different concentrations: 2 to 10 µg mL^{-1} for Co^{2+}, Fe^{3+}, and Zn^{2+}, and 4 to 20 µg mL^{-1} for Cu^{2+} and V^{4+}. Each concentration was measured in quintuplicate. Method precision was assessed by calculating the % RSDs of the detection length for both intra-day (*n* = 3), and inter-day (*n* = 6) assays. Accuracy was preliminarily evaluated by calculating the percent recovery (*n* = 6) from spiking 6 µg mL^{-1} of Zn^{2+} into tap water collected from 2 distinct sources. Additionally, the LOQ was determined based on the lowest detection distance that could be precisely determined (*n* = 3).

2.6. Applications and stability studies of the DµPADs

To assess the method's versatility, the DµPADs were tested with heavy metals including Cd, Hg, Pb, and As, commonly found in herbal supplements and cosmetics regulated by the FDA. Full method validation was performed for the determination of these metals. Accuracy was evaluated in statistical *t*-test analysis at a 95% confidence interval (*p* < 0.05), comparing results obtained from the developed DµPADs with those from ICP-OES. Each heavy metal was individually spiked into metal-free herbal supplement samples and cosmetic cream bases, as previously described in Section 2.2. Preparation of reagent, standard, and sample solutions at the concentrations following FDA limits. These solutions were analyzed in triplicate using the DµPADs. Additionally, the effect of NaCl concentration ranging from 0 to 600 mM on the determination of heavy metals was investigated to broaden the application scope by simulating conditions in seawater and salt lakes.

Furthermore, DµPADs with predeposited 5-Br-PAPS along the detection channel were kept at ambient temperature, protected from light by aluminum foil, for 8 weeks. The measurement of Co^{2+} and Zn^{2+} on DµPADs was performed in triplicate every week.

3. Results and discussion

3.1. Study of factors affecting the metal ion analysis on DµPADs

3.1.1. Selection of paper substrate. Rahbar *et al.*[36] demonstrated strong retention of dye on IE paper surfaces. However, various factors can influence the anchoring of different molecules. Therefore, the immobilization of 5-Br-PAPS was investigated on both standard cellulose paper and IE paper. Standard cellulose paper contains hydroxyl and carboxyl groups that

facilitates strong immobilization of some cationic compounds through electrostatic interactions, hydrogen bonding, van der Waals, and hydrophobic interactions.[36] IE paper comprises a cellulose substrate modified with diethylaminoethyl functional groups (pK_a = 9.5), which are protonated at neutral pH, making the paper surface an anion exchanger. The water-soluble chromogenic reagent, 5-Br-PAPS (pK_a < 1, 2.9, 11.0),[41] used for metal complexation, consists of anionic sulfonate functional groups. This reagent was applied onto both IE paper and standard cellulose paper and then immersed in the water. IE paper exhibited greater retention of 5-Br-PAP, and the histogram of the grayscale intensity of the immobilized 5-Br-PAPS on the IE paper shows better uniformity than standard cellulose paper (Fig. 1).

Both types of papers were subsequently used for DμPADs fabrication. The determination of Zn^{2+} on DμPADs fabricated from standard cellulose paper showed a longer colored distance compared to those fabricated with IE paper. Interestingly, an increase in Zn^{2+} concentration demonstrated greater changes in distance on the IE paper than on standard cellulose paper, indicating more sensitive detection. This is due to the protonated amino group on the IE paper surface, which can form ion exchange interaction with the deprotonated sulfonic group of 5-Br-PAPS. Additionally, its slightly lower flow rate than standard cellulose paper facilitated the complete colorimetric reaction of metals. In contrast, there is no specific interaction to assist the 5-Br-PAPS in anchoring to the standard paper surface (Fig. 1). Unlike cationic dyes that can be strongly retained through various interactions. Additionally, the fluid flow enabled both Zn^{2+} and un-immobilized 5-Br-PAPS to elute along the detection channel, resulting in a longer distance of color but not uniform.[36,42] However, the flow rates of these compounds may differ, and a greater amount of Zn^{2+} may flow a longer distance, which might not properly react with 5-Br-PAPS to form a color complex.

3.1.2. Effects of buffer concentration. The surface of IE paper is typically basic (~pH 8.5–9.0) due to the presence of diethylaminoethyl groups. Increasing the concentrations of acetic acid and acetic acid–Tris buffer resulted in a decrease in pH on the paper surface. For the immobilization of 5-Br-PAPS on DμPADs, the solution was prepared in varying acetic acid (10–100 mM) and acetic acid–Tris buffer (20–500 mM). The detection distance of each metal ion increased with higher concentrations of either acetic acid and acetic acid–Tris buffer (Fig. 2A and S2A†) due to the pH alteration to more acidic conditions, which promote the formation of metal ions and 5-Br-PAPS complex.[43–45] Moreover, the higher ionic strength increased competitive interactions between metal ions and the negatively charged 5-Br-PAPS immobilized on the IE paper surface.[42] Consequently, the negative charges in the buffer solution facilitated metal ions to flow a greater distance before reacting with 5-Br-PAPS, resulting in a decrease in color intensity as the buffer concentration increased.

3.1.3. Effects of 5-Br-PAPS concentration. The concentration of the metallochromic reagent can significantly affect the distance and intensity of the metal complexes. Thus, various concentrations of 5-Br-PAPS ranging from 0.25 to 1 mM
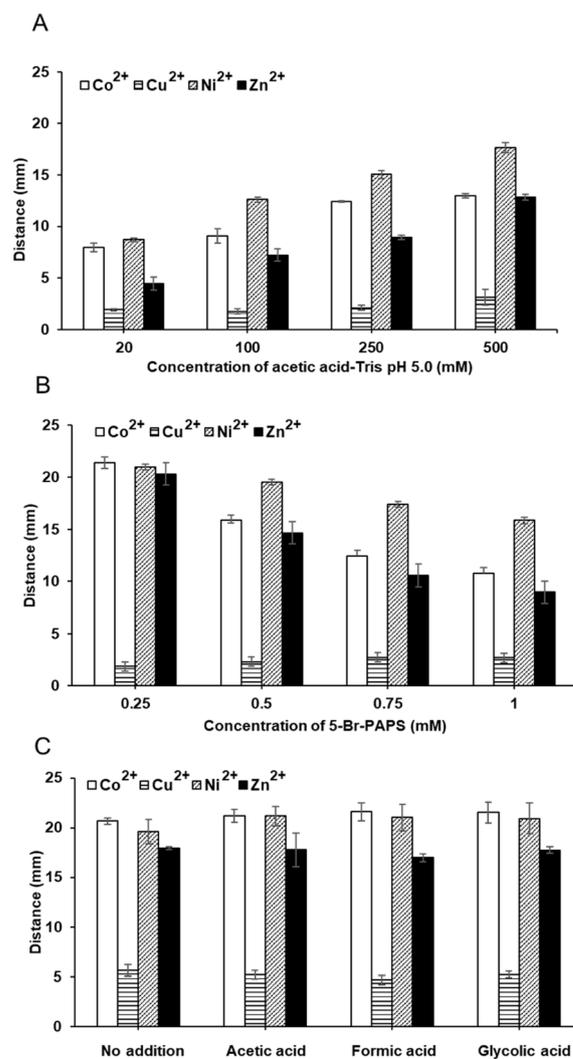

Fig. 2 Effects of (A) buffer concentration, (B) 5-Br-PAPS concentration in acetic acid–Tris pH 5.0, and (C) types of auxiliary complexing agents on the DμPADs.

dissolved in 250 mM acetic acid–Tris, and nitric acid–MES buffers were investigated. Decreasing the concentration of 5-Br-PAPS led to an increase in the distance of color change (Fig. 2B and S2B†). It can be attributed to the lower density of reagent in a certain paper area, which improves the flow of metal ions through the paper to react with the reagent. In contrast, the color intensity decreased as the concentrations of 5-Br-PAPS decreased. Hence, finding the balance between the distance and the color intensity is crucial for achieving sensitive and accurate endpoint detection.

3.1.4. Effects of auxiliary complexing agent. Metal hydrolysis typically occurs when metals are dissolved in water, especially under basic conditions where hydroxide species are abundant.[46] Consequently, most metal hydroxides are insoluble or sparingly soluble in water and the metal hydrolysis can lead to the false analytical result of some metal ions. Thus, the addition of auxiliary complexing agents could prevent metal hydrolysis.[47] Three types of auxiliary complexing agents,
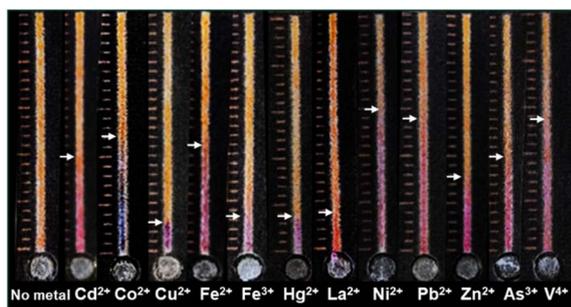
Fig. 3 Color changes of 12 heavy metal ions under the optimal conditions.

including acetic acid, formic acid, and glycolic acid, were investigated for the determination of Co^{2+}, Cu^{2+}, Ni^{2+}, and Zn^{2+}. The results show that auxiliary complexing reagents did not significantly affect the migration distance of these metals (Fig. 2C and S2C†) because all metal solutions were prepared in acidic conditions, which limits the formation of the hydroxide.

3.1.5. Screening test of different metal ions. During the optimization, 0.25 mM 5-Br-PAPS provided the highest distance of color change for 4 metal ions (*i.e.*, Co^{2+}, Fe^{2+}, Ni^{2+}, V^{4+}). Consequently, this concentration was selected for the screening of 17 metal ions. However, no additional metal ions exhibited notable response. Increasing the concentration of 5-Br-PAPS led to the detection of a greater number of metal ions. At 1 mM 5-Br-PAPS, a clear detection endpoint was observed for 12 metal ions, including Cd^{2+}, Co^{2+}, Cu^{2+}, Fe^{2+}, Fe^{3+}, Hg^{2+}, La^{2+}, Ni^{2+}, Pb^{2+}, Zn^{2+}, As^{3+}, V^{4+} (Fig. 3). Most metal complexes displayed color changes from orange-yellow to pink-purple, except for Co^{2+}, which formed a blue color complex.

This method utilizes 5-Br-PAPS for the universal detection of metal ions, providing a versatile approach applicable across a wide range of metal species. This developed device facilitates the rapid screening of metal ions, enabling efficient detection without the need for instrumentation. To enhance the specificity for targeted metal ions, further refinement of the detection protocol may be beneficial. Approaches such as the incorporation of masking reagents can be employed to selectively inhibit the reactivity of certain metal ions during detection processes, thereby allowing for the accurate detection of target metal ions. Additionally, surface-modified nanomaterials can be incorporated for the specific detection of particular types of metals.[24,25]

3.1.6. Characterization of paper surface. SEM images show no differences between the morphological characteristics of the standard and IE paper surfaces.[36] After the deposition of 5-Br-PAPS and subsequent metal binding on the paper fiber surface, the SEM images demonstrate a coating effect, resulting in a reduction of visible paper pores. Additionally, metal binding to 5-Br-PAPS produced a denser morphology and led to the disappearance of interfiber network gaps. Results obtained from SEM-EDX analysis confirmed that 5-Br-PAPS had completely formed metal complexes in areas showing color change. Elemental mapping further revealed increased signals corresponding to metal ions (*i.e.*, Cd^{2+}, Cr^{3+}, and V^{4+}) within
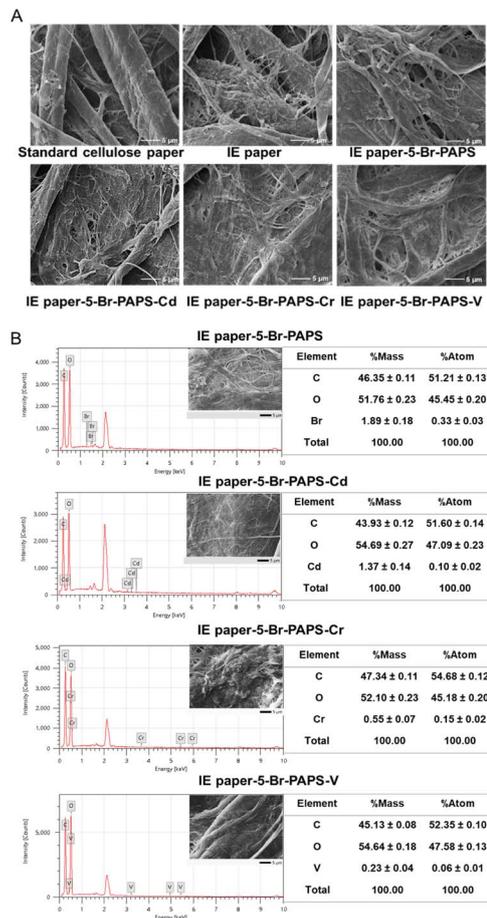

Fig. 4 Paper surface morphology and elemental analysis by (A) SEM at 10 kV with 3000 magnifications and (B) SEM-EDX at 15 kV with 3000 magnifications, respectively.

these color-altered regions, demonstrating successful complexation at the microstructural level (Fig. 4). Although Cr^{3+} did not exhibit a clear detection endpoint under optimized conditions, a color change from complexation was observed at higher concentrations of 5-Br-PAPS.

The IR spectra illustrated the N–H and C–H stretching vibration bands for both IE paper and 5-Br-PAPS immobilized on IE paper at 3333 cm^{-1}, 3288 cm^{-1}, and 2928 cm^{-1}, respectively. After binding with Hg^{2+}, these bands slightly shifted to 3339 cm^{-1} and 3281 cm^{-1}. The N=N and C–N stretching vibrations of 5-Br-PAPS were displayed at 1427 and 1310 cm^{-1}, respectively. Additionally, the C–O stretching bands were observed at 1055 cm^{-1} and 1109 cm^{-1}, indicating the presence of dimethylaminoethyl cellulose in the IE paper. Notably, C–O bands were observed in both 5-Br-PAPS and the metal-bound 5-Br-PAPS. The intensity of these bands increased after binding with the heavy metal, suggesting that the interaction may stabilize certain functional groups and influence their vibrational frequencies (Fig. 5).[48]

3.2. Method validation

Calibration curves were established by plotting the migration distance against concentrations ranging from 2 to 10 μg per mL
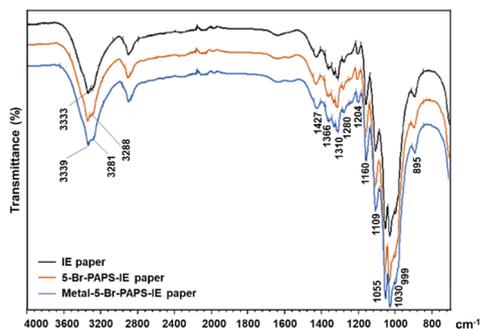
Fig. 5 Comparison of IR spectra depicted the surface functionalization of an IE paper surface with 5-Br-PAPS and metal binding.

Table 2 Calibration curve of Co^{2+}, Cu^{2+}, Fe^{3+}, V^{4+} and Zn^{2+}

Metal ion	Linear range ($\mu g\ mL^{-1}$)	Equation	r^2	% RSD
Co^{2+}	2–10	$0.7732x + 5.8012$	0.9899	3.0–5.7
Cu^{2+}	4–20	$0.2173x + 2.7744$	0.9851	3.7–7.8
Fe^{3+}	2–10	$0.8613x + 4.7834$	0.9950	1.7–4.8
V^{4+}	4–20	$0.3577x + 2.7576$	0.9907	3.1–6.5
Zn^{2+}	2–10	$0.7831x + 5.3519$	0.9958	1.1–6.5

Co^{2+}, Zn^{2+}, and Fe^{3+}, and from 4 to 20 $\mu g\ mL^{-1}$ for Cu^{2+} and V^{4+}. The response of all metal ions fitted the linear regression model with r^2 ranging from 0.9851 to 0.9958. The intra-day precision showed RSDs in the range of 1.1 to 7.8% (Table 2 and Fig. S3†). The accuracy of the method was presented in terms of percent recovery. Tap waters collected from 2 sources were spiked with a 6 μg per mL Zn^{2+} solution, resulting in percent recoveries ranging from 100.3 ± 3.5 to 104.5 ± 3.8. This indicates that there was no interference from sample matrices affecting the detection method.

3.3. Applications and stability studies of the DµPADs

Results obtained from the DµPADs and ICP-OES for the analysis of As and Pb in cream and herbal supplements and Cd in cream base were not significantly different at the 95% confidence interval. However, the Cd and Hg in cream and herbal samples cannot be detected on the DµPADs due to their concentrations being lower than the LOQs (Table 3).

To broaden the applications of the DµPADs, the effects of dissolved salt in artificial seawater and salt lakes were investigated through the determination of Zn^{2+} and Co^{2+} as model analytes. Such conditions, which typically contain dissolved salts at approximately 600 mM, predominantly consisting of Na^+ and Cl^- ions.[38] Consequently, NaCl concentrations ranging from 10 to 600 mM were investigated. Compared to the previous report, the spot of anionic fluorescein was eluted using 200 mM NaCl as the eluent. It confirms that immobilization is based on a reversible ion exchange mechanism.[36] Other studies reported that high salt content could potentially extend the color development due to weaker electrostatic interactions between target analytes and reagents with high ionic strength.[42,49]

Interestingly, increasing the amount of NaCl to 600 mM did not significantly alter the length of color change across the entire NaCl concentration range, nor in its absence (Fig. S4†). This can be attributed to the stronger binding affinity of 5-Br-PAPS toward transition metals compared to alkaline metal (Na^+), suggesting that electrostatic interaction does not interfere with coordinate covalent interaction after the metal complex formation. Additionally, NaCl may elute the free 5-Br-PAPS, but the presence of heavy metal ions can prompt rapid complex formation, altering their solubility. These promising results demonstrated the capability of the proposed DµPADs for detecting Zn^{2+} and Co^{2+} in samples containing high salt concentrations, such as seawater or salt lakes samples. However, environmental water samples present complex matrices, posing challenges, particularly in terms of background color interference in analyses with the proposed DµPADs. Several approaches effectively address this issue. Sample filtration removes particulates and suspended solids contributing to background color, while sample dilution lowers interfering substance concentrations. Solid-phase extraction (SPE) further minimizes color interference. Additionally, acid digestion with concentrated nitric or hydrochloric acid decomposes organic matter, dissolves metals, and reduces turbidity, clarifying the sample and enhancing signal accuracy by isolating target metals—an approach widely used in preparing complex samples for metal analysis.

Moreover, the DbD of Co^{2+} and Zn^{2+} using the predeposited 5-Br-PAPS on the detection channel of the DµPADs was evaluated under ambient temperature storage. Results indicated that the DµPADs were stable for at least 8 weeks, which would be a great potential for the in-field analysis (Fig. 6).

Table 3 Applications of DµPADs for the determination of heavy metals in cosmetics and herbal supplements

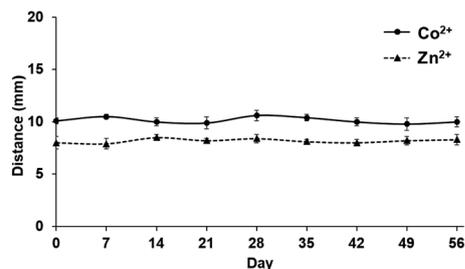| Metal	Sample	The proposed method ($\mu g\ mL^{-1}$)	ICP-OES ($\mu g\ mL^{-1}$)	p-value	FDA limit Cosmetics	Herbal supplement
As	Cream	5.5 ± 0.8	5.1 ± 0.3	0.30	5	4
	Herbal capsules	4.7 ± 0.6	4.5 ± 0.4	0.23		
Pb	Cream	19.8 ± 0.5	20.3 ± 0.1	0.16	20	10
	Herbal capsules	12.4 ± 0.7	11.8 ± 0.2	0.17		
Cd	Cream	3.5 ± 0.9	3.1 ± 0.2	0.43	3	0.3
	Herbal capsules	ND	0.3 ± 0.0	0.00		
Hg	Cream	ND	1.1 ± 0.3	0.01	1	—

Fig. 6 Stability study of the predeposited reagent on DμPADs stored at ambient temperature for the determination of Co^{2+} and Zn^{2+}.

4. Conclusions

This work focused on the determination of heavy metal ions using DμPADs, which rely on the color complex formation between metal ions and 5-Br-PAPS. The anionic exchange paper exhibited superior performance compared to cellulose paper in terms of detection sensitivity, color uniformity, and accurate detection endpoint readout. This suggests that IE interactions can enhance analytical performance, specifically for immobilizing anionic water-soluble compounds on IE paper.

The method was evaluated for detecting 17 species of metal ions, with 12 metal ions successfully detected. It was applied for the rapid visual screening of toxic metals commonly found in herbal supplements and cosmetics regulated by the FDA. Importantly, the method proved robust under simulated conditions of seawater and salt lakes with high NaCl concentrations, showing that the affinity of 5-Br-PAPS and the flow rate of heavy metals remained unaffected. This method demonstrates the potential of DμPADs as an alternative approach with distinct advantages such as simplicity, cost-effectiveness, and suitability for resource-limited areas. Additionally, the method was evaluated using the green analytical chemistry criteria and achieved an AGREE score of 0.65, highlighting the method's environmental sustainability and practical applicability.

The proposed method effectively detects heavy metals in the ppm range ($\mu g\ mL^{-1}$), with applications for identifying toxic heavy metals in cosmetic and herbal supplements yielding results comparable to FDA-approved standard methods. Therefore, the proposed method meets the detection limit requirements for specific field-based applications. However, it may not detect all 12 heavy metal ions across various real-world scenarios, as acceptable limits differ by metal type and sample matrix. Future enhancements for field use could focus on optimizing sensitivity through adjustments in reagent concentration and sample preconcentration methods. Additionally, incorporating nanoparticle-based amplification techniques may facilitate lower limits of detection, enhancing the assay's applicability for trace heavy metal detection in diverse environmental conditions.

Data availability

The data supporting this article have been included as part of the ESI.†

Author contributions

Yanawut Manmana: data curation; formal analysis; funding acquisition; investigation; methodology; software; validation; visualization; writing – original draft; and writing – review & editing. Mirek Macka: conceptualization; resources; supervision; and writing – review & editing. Nantana Nuchtavorn: conceptualization; data curation; formal analysis; funding acquisition; investigation; methodology; project administration; resources; software; supervision; validation; visualization; writing – original draft; and writing – review & editing.

Conflicts of interest

There are no conflicts to declare.

Acknowledgements

References

1 J. Briffa, E. Sinagra and R. Blundell, *Heliyon*, 2020, **6**, e04691.
2 P. B. Tchounwou, C. G. Yedjou, A. K. Patlolla and D. J. Sutton, *Exper. Suppl.*, 2012, **101**, 133–164.
3 United States Pharmacopeial Convention, <233> Elemental Impurities – Procedures, in *United States Pharmacopeia and National Formulary*, United States Pharmacopeial Convention, Rockville, MD.
4 U.S. EPA, *Method 200.7: Determination of Metals and Trace Elements in Water and Wastes by Inductively Coupled Plasma-Atomic Emission Spectrometry*, Revision 4.4, Cincinnati, OH, 1994, https://www.epa.gov/sites/default/files/2015-06/documents/epa-200.7.pdf.
5 ISO 21392:2021-Measurement of traces of heavy metals in cosmetic finished products using ICP/MS technique, https://www.iso.org/standard/70854.html.
6 Y. Lin, D. Gritsenko, S. Feng, Y. C. Teh, X. Lu and J. Xu, *Biosens. Bioelectron.*, 2016, **83**, 256–266.
7 N. Nuchtavorn and M. Macka, *Anal. Chim. Acta*, 2016, **919**, 70–77.
8 Y. Manmana, B. Chutvirasakul, L. Suntornsuk and N. Nuchtavorn, *Pharm. Sci. Asia*, 2019, **46**, 270–277.
9 N. Khunkitchai, N. Nuchtavorn, T. Rypar, M. Vlcnovska, L. Nejdl, M. Vaculovicova and M. Macka, *Chem. Eng. J.*, 2022, **428**, 132508.
10 X. Gong, J. Shao, S. Guo, J. Pan and X. Fan, *J. Pharm. Anal.*, 2021, **11**, 603–610.
11 N. Nuchtavorn, J. Leanpolchareanchai, L. Suntornsuk and M. Macka, *Anal. Chim. Acta*, 2020, **1098**, 86–93.
12 M. Vodova, L. Nejdl, K. Pavelicova, K. Zemankova, T. Rrypar, D. Skopalova Sterbova, J. Bezdekova, N. Nuchtavorn, M. Macka, V. Adam and M. Vaculovicova, *Food Chem.*, 2022, **380**, 132141.

13 L. L. Shen, G. R. Zhang and B. J. M. Etzold, *ChemElectroChem*, 2020, **7**, 10–30.

14 Y. Zhang, L. Qian, Z. Yu, Y. Yu, C. Feng, L. Niu and J. Zhang, *Microchem. J.*, 2024, **196**, 109652.

15 S. H. Al-Jaf, S. S. Mohammed Ameen and K. M. Omer, *Lab Chip*, 2024, **24**, 2306–2316.

16 R. B. R. Mesquita, C. Klima, H. Martínez-Pérez-Cejuela, A. R. Monforte, A. C. S. Ferreira and A. O. S. S. Rangel, *Microchem. J.*, 2023, **188**, 108462.

17 P. Aryal, E. Brack, T. Alexander and C. S. Henry, *Anal. Chem.*, 2023, **95**, 5820–5827.

18 B. Jin, Z. Li, G. Zhao, J. Ji, J. Chen, Y. Yang and R. Xu, *Anal. Chim. Acta*, 2022, **1192**, 339388.

19 R. Silva, A. Ahamed, Y. H. Cheong, K. Zhao, R. Ding and G. Lisak, *Anal. Chim. Acta*, 2022, **1197**, 339495.

20 P. Abdollahiyan, M. Hasanzadeh, F. Seidi and P. Pashazadeh-Panahi, *J. Environ. Chem. Eng.*, 2021, **9**, 106197.

21 Q. Miao, J. Qi, Y. Li, X. Fan, D. Deng, X. Yan, H. He and L. Luo, *Analyst*, 2021, **146**, 6297–6305.

22 L. Zhu, X. Lv, Z. Li, H. Shi, Y. Zhang, L. Zhang and J. Yu, *Biosens. Bioelectron.*, 2021, **192**, 113524.

23 P. Kamnoet, W. Aeungmaitrepirom, R. F. Menger and C. S. Henry, *Analyst*, 2021, **146**, 2229–2239.

24 M. Wang, Z. Song, Y. Jiang, X. Zhang, L. Wang, H. Zhao, Y. Cui, F. Gu, Y. Wang and G. Zheng, *Anal. Bioanal. Chem.*, 2021, **413**, 3299–3313.

25 Y. Zhang, Y.-L. Li, S.-H. Cui, C.-Y. Wen, P. Li, J.-F. Yu, S.-M. Tang and J.-B. Zeng, *J. Anal. Test.*, 2021, **5**, 11–18.

26 J. Zhou, B. Li, A. Qi, Y. Shi, J. Qi, H. Xu and L. Chen, *Sens. Actuators, B*, 2020, **305**, 127462.

27 X. Xiong, J. Zhang, Z. Wang, C. Liu, W. Xiao, J. Han and Q. Shi, *BioChip J.*, 2020, **14**, 429–437.

28 Y. Guan and B. Sun, *Microsyst. Nanoeng.*, 2020, **6**, 14.

29 J. P. Devadhasan and J. Kim, *Sens. Actuators, B*, 2018, **273**, 18–24.

30 J. C. Hofstetter, J. B. Wydallis, G. Neymark, T. H. Reilly Iii, J. Harrington and C. S. Henry, *Analyst*, 2018, **143**, 3085–3090.

31 L. Cai, Y. Fang, Y. Mo, Y. Huang, C. Xu, Z. Zhang and M. Wang, *AIP Adv.*, 2017, **7**, 085214.

32 D. M. Cate, S. D. Noblitt, J. Volckens and C. S. Henry, *Lab Chip*, 2015, **15**, 2808–2818.

33 B. Chutvirasakul, N. Nuchtavorn, M. Macka and L. Suntornsuk, *Anal. Bioanal. Chem.*, 2020, **412**, 3221–3230.

34 B. Chutvirasakul, N. Nuchtavorn, L. Suntornsuk and Y. Zeng, *Electrophoresis*, 2020, **41**, 311–318.

35 N. Nuchtavorn, T. Rypar, L. Nejdl, M. Vaculovicova and M. Macka, *Trends Anal. Chem.*, 2022, **150**, 116581.

36 M. Rahbar, A. R. Wheeler, B. Paull and M. Macka, *Anal. Chem.*, 2019, **91**, 8756–8761.

37 F. Pena-Pereira, W. Wojnowski and M. Tobiszewski, *Anal. Chem.*, 2020, **92**, 10076–10082.

38 F. J. Millero, R. Feistel, D. G. Wright and T. J. McDougall, *Deep Sea Res., Part I*, 2008, **55**, 50–72.

39 A. Bendre, M. P. Bhat, K.-H. Lee, T. Altalhi, M. A. Alruqi and M. Kurkuri, *Mater. Today Adv.*, 2022, **13**, 100205.

40 AOAC, *Guidelines for Dietary Supplements and Botanicals*, 2019.

41 K. U. Kuang Lu Cheng, T. Imamura, *CRC Handbook of Organic Analytical Reagents*, CRC Press, 2019.

42 K. Yamada, T. G. Henares, K. Suzuki and D. Citterio, *ACS Appl. Mater. Interfaces*, 2015, **7**, 24864–24875.

43 D. Horiguchi, M. Saito, K. Noda and K. y. Kina, *Anal. Sci.*, 1985, **1**, 461–465.

44 S. Motomizu, M. Oshima, M. Kuwabara and Y. Obata, *Analyst*, 1994, **119**, 1787–1792.

45 G. Deng and G. E. Collins, *J. Chromatogr. A*, 2003, **989**, 311–316.

46 P. L. Brown and C. Ekberg, *Hydrolysis of Metal Ions—Theory*, Wiley-VCH Verlag GmbH & Co. KGaA, 2016.

47 D. A. Skoog, D. M. West, S. R. Crouch and F. J. Holler, *Fundamentals of Analytical Chemistry*, Brooks/Cole, Cengage Learning, 2014.

48 A. Raj, R. M. Rego, K. V. Ajeya, H.-Y. Jung, T. Altalhi, G. M. Neelgund, M. Kigga and M. D. Kurkuri, *Chem. Eng. J.*, 2023, **453**, 139757.

49 T. Rypar, V. Adam, M. Vaculovicova and M. Macka, *Sens. Actuators, B*, 2021, **341**, 129999.